

Wireless Double Micro-Resonator for Orientation Free Tracking of MR-Catheter During Interventional MRI

Omar Nassar¹, Dario Mager, and Jan G. Korvink¹, *Senior Member, IEEE*

Abstract—Interventional magnetic resonance imaging (iMRI) using MR-catheters has been explored during the past decade because of its potential impact on the field of minimally invasive medical procedures, especially applied to vascular diseases. Tracking the catheter’s tip during an iMRI procedure using active electronic components has major benefits but still faces challenges regarding safety and the quality of visualization, which has prevented its clinical use up to now. Here we propose a novel micro detector with a total length of 8 mm built upon a flexible substrate with a total thickness of less than $60\ \mu\text{m}$. The design of the detector is based on two perpendicularly oriented saddle coils that together create a homogeneous magnetic field when wrapped onto the catheter tube, thus maintaining constant visibility of the catheter under rotation, with practically no dead angle. Being self-resonant, the proposed detector allows wireless tracking of the catheter position, whilst preventing any heating hazard due to the absence of radiofrequency cables. The micro-resonator was fabricated using a multilayer flexible electronics fabrication process.

Index Terms—Electromagnetic coupling, electromagnetic fields, engineering in medicine and biology, magnetic resonance imaging, radiofrequency microelectromechanical systems.

I. INTRODUCTION

CARDIOVASCULAR diseases have been reported as the leading cause of death worldwide over the past twenty years, with more than 17 million deaths in 2017 surpassing all other medical causes combined [1]. Catheter-based intervention is one of the major approaches used in the diagnosis and treatment of heart diseases [2], [3], it also plays an important role in the field of minimally invasive medicine. Providing a surgeon with an accurate geometrical orientation of the catheter’s tip relative to the patient’s body is a prerequisite for the further development of minimally invasive medical interventions. X-ray guided catheters suffer from poor contrast of soft tissues, which makes the method critical for complex interventional procedures [2]. Hence, the geometrical tracking of a catheter’s tip

Manuscript received February 18, 2020; revised April 21, 2020; accepted July 13, 2020. Date of publication July 17, 2020; date of current version February 19, 2021. This work was supported by the DAAD-GERLS program and the European Union (H2020-FETOPEN-1-2016-2017-737043-TISuMR). This paper is an extension from a presentation at the 2019 IEEE Sensors Conference held in Montreal Canada on October 27-30 2019. (*Corresponding author: Jan G. Korvink.*)

The authors are with the Institute of Microstructure Technology (IMT), Karlsruhe Institute of Technology (KIT), 76344 Eggenstein-Leopoldshafen, Germany (e-mail: omar.nassar@kit.edu; dario.mager@kit.edu; jan.korvink@kit.edu).

Digital Object Identifier 10.1109/JERM.2020.3010093

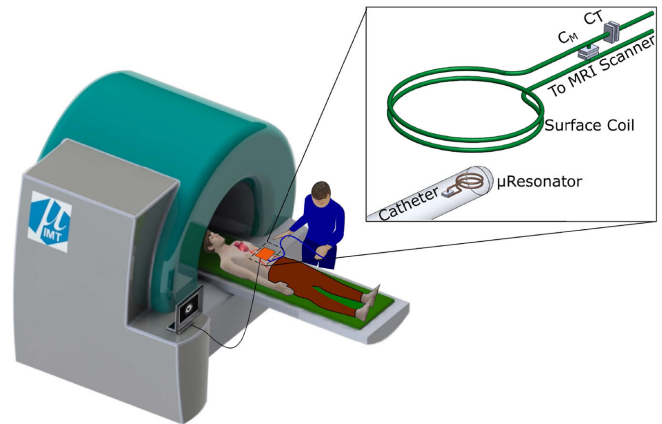


Fig. 1. Minimally invasive operation under interventional Magnetic Resonance Imaging (iMRI) through inductive coupling.

within an MR environment has been a topic of extensive attention during the past decade [4], [5]. The catheter can be visualized in the MR environment employing one of two techniques. The first passive technique uses relaxation contrast agents [6] and still lacks reliability [7]. The second technique is electrically active, requiring supplemental hardware such as radio frequency (RF) antennas [8], [9] or resonators [10], [11], which are placed on the tip of the catheter, resulting in a traceable bright spot in the MR image. Micro-resonators are known to have a higher signal-to-noise ratio (SNR) than RF antennas, since RF antennas possess long loopless wire leads with high impedance that ultimately lead to a loss of signal. By tuning the micro-resonator to the Larmor frequency of any abundant nucleus, and continuously subjecting it to radio frequency excitation pulses, the catheter’s motion can be tracked in real-time under direct image guidance. Using cables for tuning and transmitting the micro-coil signal is known to cause dangerous tissue heating, leading to safety hazards during iMRI procedures [12], [13], and hence preventing this technology to find widespread use.

An alternative approach is to wirelessly couple the resonator on the catheter’s tip, through inductive coupling to a surface coil outside the patient [14]–[16]. The surface coil is conventionally connected to a matching and tuning circuit, as well as to the MRI scanner as shown in Fig. 1. Tracking the catheter in this way has proven to be reliable, delivering high contrast visualization [15]. However, as the orientation of the catheter changes, the visibility

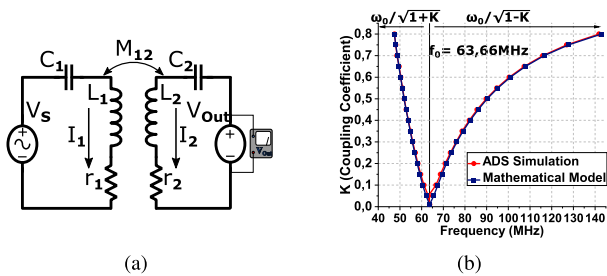


Fig. 2. (a) Equivalent schematic circuit of two inductively coupled resonators. (b) Degree of splitting of the resonance frequency versus coupling coefficient (K). The analytical formula is compared to an ADS simulation, reproduced with permission from [21] ©2019 IEEE.

changes and can be lost when the B_1 field of the micro-resonator and the surface coil are nearly orthogonal [15], [17]. Also, as the coupling varies with motion and orientation, the entire system needs to be re-matched and tuned. Moreover, resonance frequency splitting occurs when two closely tuned inductors are inductively coupled [18].

In this study, we propose a micro-resonator design based on a double saddle coil, which maintains almost constant coupling between the resonator on the catheter's tip and the external surface coil throughout the different axial orientations. A design of the double resonator was fabricated on a flexible substrate using one of two multilayer fabrication processes. One method is based on a conventional lithography process for high-resolution structures and is mass production capable [19], the other process uses inkjet printing for fast prototyping [20]. The enhancement provided by the proposed double coil design over a conventional single-coil is presented using multiphysics simulations of the radiofrequency fields, and is verified experimentally.

II. THEORY

The angular resonance frequency ω_0 of a lumped-parameter RF resonator is based on its inductance L and capacitance C and is given by $\omega_0 = \sqrt{1/LC}$. If two coils are in close proximity to each other they become inductively coupled and share a mutual inductance, as shown in Fig. 2(a), thereby the resonance frequency of each coil is shifted away from its initial value by an amount that depends on the strength of the coupling. In case both of the resonators are tuned to the same resonance frequency, i.e. $\omega_0 = \omega_{01} = \omega_{02}$, then splitting of this frequency will occur, resulting in two frequencies ($\omega_{1,2}$) shifted to the right and left of the original value [21]:

$$\omega_{1,2} = \frac{\omega_0}{\sqrt{1 \pm K}}, \quad (1)$$

where K is the coupling coefficient, which depends on the mutual inductance between the two inductors according to $K = M\sqrt{L_1L_2}$. Equation (1) is derived in the appendix. The frequency splitting for two inductively coupled resonators was simulated using Agilent's Advanced Design System (ADS). Each resonator has a resonance frequency of $\omega_0 = 63.6$ MHz. The coupling coefficient was swept and the results were compared to the mathematical model as shown in Fig. 2(b).

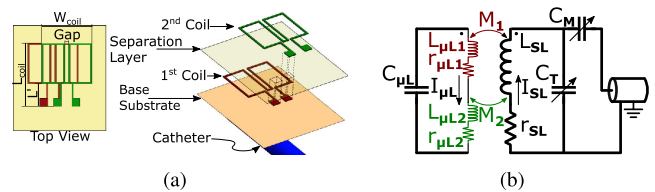


Fig. 3. (a) Illustration for the double saddle coil design. (b) Equivalent schematic circuit for the coupling between a surface pickup coil and the tuned double saddle coil.

A. Micro-Resonator Design

The image from a single catheter micro coil convolutes the NMR signal with orientation of the coil. As the axial orientation of the catheter changes w.r.t. the static receiver coil, the coupling coefficient is altered. Moreover, the coupling can be totally lost when the B_1 fields of the micro-resonator and surface coil are nearly orthogonal. Therefore, we propose a micro-resonator design based on two orthogonal saddle coils, as shown in Fig. 3(a), which maintains near-constant coupling under rotation of the catheter. The two saddle coils have their B_1 -fields arranged orthogonally, which largely decouples them, and are connected in series and tuned to the Larmor frequency by a single capacitor, as shown in Fig 3(b). To connect the surface coil to the MRI scanner, its impedance has to match the impedance of the transmitting cable (50Ω). This is achieved through a matching and tuning circuit as shown in Fig. 3(b), where C_T is used for tuning as well as to set the real part of the impedance to 50Ω , while the residual imaginary part is eliminated by matching with C_M [21].

B. Simulation

To gain insight into the magnetic field distribution generated by saddle coils in the space around the catheter tube, and to measure angular dependence of coupling with the surface coil, the setup was simulated using the finite element analysis software COMSOL Multiphysics. Two simulation scenarios were considered:

- 1) A micro saddle coil connected to a 50Ω port for excitation. The magnetic flux density was determined, as shown in Fig. 4. Single and double saddle coils were simulated, and in each case, the gap was swept to obtain the best distribution of the magnetic field.
- 2) The second simulation model had a surface coil connected to the excitation port, and a saddle coil was connected to a port for measuring the induced voltage, as shown in Fig. 5(a). Single and double saddle coils were simulated, and in each case, the three possible relative orientations between the saddle coil and the surface coil were swept from 0° to 360° . For both models, the COMSOL radio-frequency module was used, and simulations were executed at an excitation frequency of 63 MHz.

As part of the simulation environment, the saddle coils were located inside a box-shaped domain to model the surrounding

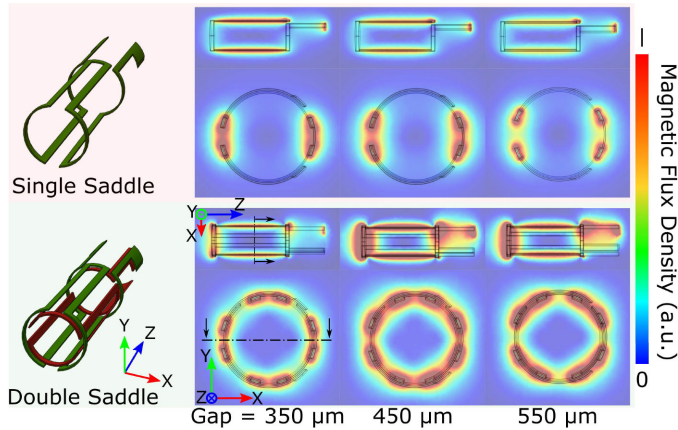


Fig. 4. Magnetic flux density generated by the saddle coils excited at 63 MHz is plotted. The top row shows the magnetic flux generated by a single saddle coil at two different cross-sections views, one perpendicular to the axis of the coil and the other along its axis. The bottom row shows the magnetic flux generated by a double saddle coil. The magnetic flux is plotted at different gaps to show the change in its distribution.

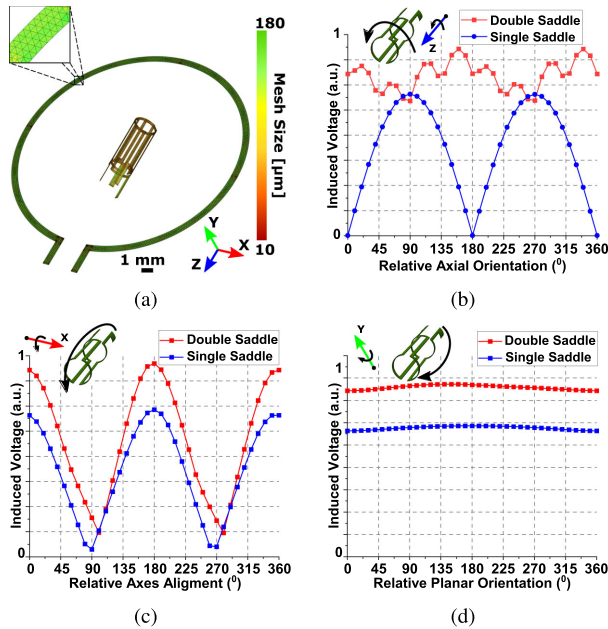


Fig. 5. (a) Inset shows the refined tetrahedral mesh used for the numerical model, which in turn contains the micro saddle coil placed within the loop of a surface coil. The curves show the induced voltage in the saddle coil due to the surface coil, versus the three orthogonal relative rotations: (b) axial orientation of the saddle coil, (c) alignment of the axes of surface and saddle coil, and (d) in-plane rotation of the saddle coil.

sample (water), which in turn was placed inside a larger box-shaped domain to model the surrounding air. To prevent back-scattering, a radiation boundary condition was added, which acted as an absorbing layer. The free tetrahedral mesh was refined to resolve the structure correctly, as shown in Fig. 5(a).

The results of the first model revealed that the double coil provided more sources of magnetic flux around the coils than the single coil, as shown in Fig. 4. The generated magnetic field's distribution around the coils can be controlled by changing the gap distance between the two loops of the saddle coils. With

TABLE I
DOUBLE SADDLE COIL'S DIMENSIONS (USED IN THE COMSOL SIMULATION AS WELL AS FOR FABRICATION)

L_{coil} [mm]	W_{coil} [mm]	L' [mm]	Gap [μm]	Track _w [μm]
8	5	3	450	200

fixing the dimensions to the values listed in Table I and sweeping the gap, it was found that a gap of 450 μm provided the best homogeneity for the magnetic field. Hence, this gap value was used for further simulation and fabrication.

Fig. 5(b)–(d) show the results of the second simulation model. The change in the relative axial orientation is Fig. 5(b). For a single saddle coil, the coupling was maximum when its B_1 field aligned with the surface coil's field, and then the coupling decreased as the relative angle between the fields increased. When a perpendicular position was taken on, no coupling was observed. In the case of a double coil, the coupling persisted throughout the entire range of relative axial orientations, with values varying about the maximum value achieved by the single saddle coil. The change in the relative angle between the coils' axes is shown in Fig. 5(c). In both cases of the single and double saddles, the maximum coupling occurs when the saddle coil's axis is perpendicular to the surface coil's axis, and minimum coupling was observed when the axes coincided. Fig. 5(d) shows that the coupling doesn't change much as the micro detector orients in the 2D plane. During invasive medical operations, it's expected that the catheter is intensively subjected to rotations along its axis, and to rotations in the plane of the surface coil (along the length of a laying body, and across its width), and that the angle between the coils' axes seldom changes with large angles (into the depth of the body). Hence, the double saddle coil is considered optimum for the catheter application.

III. FABRICATION

Fabricating a micro double saddle coil around a slender catheter tube is a challenging task since it requires a 3D micro fabrication process. The fabrication is facilitated by 2D patterning of conductive layers on both sides of a thin planar polymer film. Then the 3D structure is achieved by rolling the film around a catheter tube [19]. Patterning of the conductive layers has been done using both inkjet printing, and photolithographic patterning. Direct metal inkjet printing is a fast and efficient way for prototyping, but has a low resolution (above 50 μm) and is not yet suitable for mass production. Photolithography, on the other hand, is more costly but offers a high enough resolution and is suitable for mass production at the wafer scale.

A. Inkjet Printing

Kapton films (Dupont) with a thickness of 25 μm offered sufficient rigidity for mechanical handling and was flexible enough to be rolled around a catheter. The printing was performed using a FUJIFILM Dimatix DMC-2800 printer, loaded with 10 pL cartridge (DMC-11610, FUJIFILM Dimatix). The cartridge was filled with silver nanoparticle ink with a particle

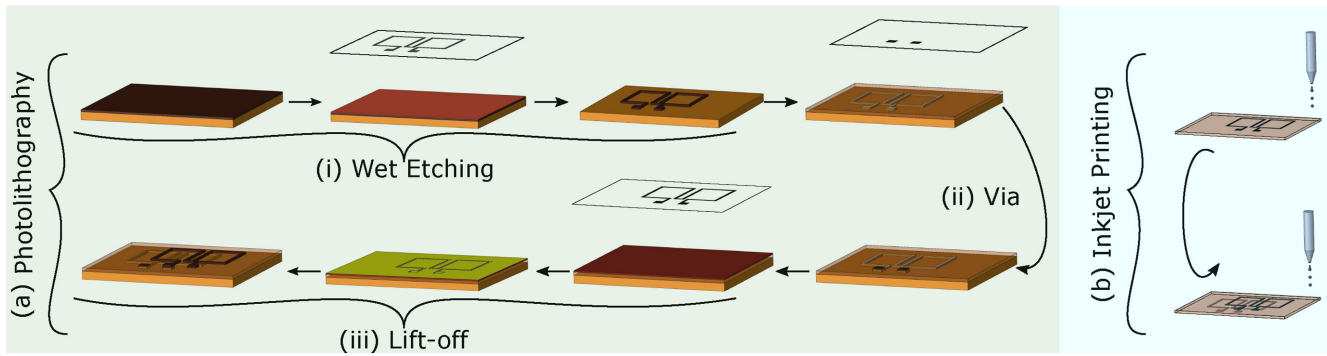


Fig. 6. Schematic illustration of the process flow for both metal track fabrication techniques. (a) Photolithography process with three main steps. (i) Wet etching of the first conductive layer after resist patterning. (ii) Separation layer possessing via using UV sensitive liquid polyimide. (iii) Deposition of the second conductive layer using a standard Lift-off process. (b) Inkjet printing of conductive ink on both sides of the Kapton film.

diameter ≤ 50 nm (Sigma-Aldrich). The ink is rated at room temperature with a surface tension of 35 mN m^{-1} to 40 mN m^{-1} and a viscosity of 10 mPa sec to 18 mPa sec . The printer head and the substrate were maintained at room temperature during printing. The drop spacing was set to $40 \mu\text{m}$, and the printing frequency to 5 kHz . Before printing, the polymer film was cleaned with acetone, isopropyl alcohol (IPA), and deionized water (DI water). Printing was done in two steps as shown in Fig. 6(b). The first layer was printed, then the substrate was transferred for drying to a hot plate set at 90°C for 15 min. Subsequently, the substrate was flipped over, and after the second layer was printed, it was dried again on a hotplate at 90°C for 15 min. Lastly, the structures were sintered in an oven at 150°C for 1 h.

B. Photolithography

The photolithography process was performed in three main steps, as illustrated in Fig. 6 a. The first layer pattern was formed by chemical wet etching (Fig. 6 a(i)). The base substrate was a $25 \mu\text{m}$ thick polyimide sheet, laminated from one side with $9 \mu\text{m}$ thick copper (AkaFlex KCL 2-9/25 HT, Krempel GmbH). The sheet was initially cut to the shape of a 100 mm wafer with an infrared laser cutter (VLS3.50, Universal Laser System), then laminated onto a silicon wafer pre-coated with $3.3 \mu\text{m}$ AZ4533 positive photoresist (MicroChemicals GmbH) at 4000 rpm for handling purposes. The wafer was transferred to a hotplate for baking at 95° for 1 min. The wafer was then immersed for 30 sec in a sodium persulfate solution ($\text{Na}_2\text{S}_2\text{O}_8$, 240 gL^{-1}) to etch the copper surface to promote photoresist adhesion. A $3.3 \mu\text{m}$ layer of AZ4533 resist was spin-coated onto the film. After soft-baking at 95°C for 1 min the photoresist was structured by UV exposure at a dose of 235 mJcm^{-2} . The photoresist was developed in a KOH-based AZ400K developer, prepared at 1:4 dilution, for 3 min, and subsequently cleaned with DI water. The exposed copper was removed by wet etching in a sodium persulfate solution, after which the remaining photoresist was stripped using acetone. The second main step (ii) formed the vias that connected the bottom and top metal layers, as shown in Fig. 6 a(ii). On the top of the structured Kapton film, a $20 \mu\text{m}$ layer of liquid polyimide LTC9310 (FUJIFILM electronic materials) was spin-coated at 1700 rpm . After soft-baking at 100°C for

4 min, the photoresist was structured by UV exposure at a dose of 550 mJcm^{-2} . Then the sample was continuously sprayed by QZ3512 (FUJIFILM electronic materials) for development. The sample was transferred to a vacuum oven set to 350° for a duration of 1 h, to cure the polyimide into a flexible film with a thickness of around $10 \mu\text{m}$. On top of the cured film, the second metal layer was defined using a lift-off process, as shown in Fig. 6 a(iii). A $2 \mu\text{m}$ layer of negative photoresist ma-N 1420 (Micro Resist Technology GmbH) was spin-coated on the top of the cured film at 3000 rpm . After baking at 100°C for 2 min, the photoresist was structured by UV exposure at a dose of 580 mJcm^{-2} . The sample was developed in ma-D 533/S for 3 min and cleaned with DI water. A 20 nm chromium and 60 nm gold layer was deposited using physical vapour deposition (PVD), at the deposition rate of 0.5 nm/sec and 0.8 nm/sec , respectively. The sacrificial photoresist was stripped off for 15 min with acetone, followed by rinsing with DI water.

C. Electrodeposition and Rolling

For radio frequency applications, a minimum thickness of the conductive traces is required based on the working frequency, to maintain a low enough RF resistance. The effective skin depth δ of the conductor can be calculated using $\delta = \sqrt{\rho/\pi f \mu}$, where f is the electrical signal's frequency, and ρ and μ are the resistivity and permeability of the conductor material. In the case of inkjet printing, the printed inks contain large amounts of solvent, therefore after sintering, this results in tracks with thicknesses in the range of hundreds of nanometers. Also, in the case of photolithography, the deposited seed layer is only 100 nm thick. The height of the tracks is therefore increased via electroplating. However, electroplating of conductive tracks onto a flexible substrate is challenging as film stress can result in the tracks peeling off. Plating was done using a home-built power source [22], which allows controlling the microstructure of the deposited copper layer through pulsed electroplating. A first rough copper layer was deposited to promote adhesion, then a smooth $10 \mu\text{m}$ thick layer was deposited to decrease resistance, maintaining a roughness of around 30 nm . Finally, the film with the completed saddle coil was rolled around a $5 \text{ fr} = 1.667 \text{ mm}$ diameter catheter tube using a process reported previously [19].

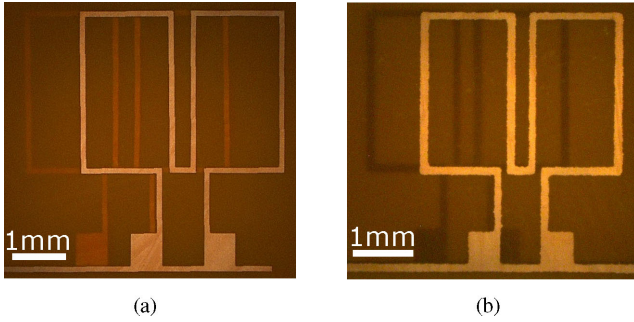


Fig. 7. Microscope images of the 2D patterned double saddle coil fabricated by (a) the lithography process and (b) inkjet printing.

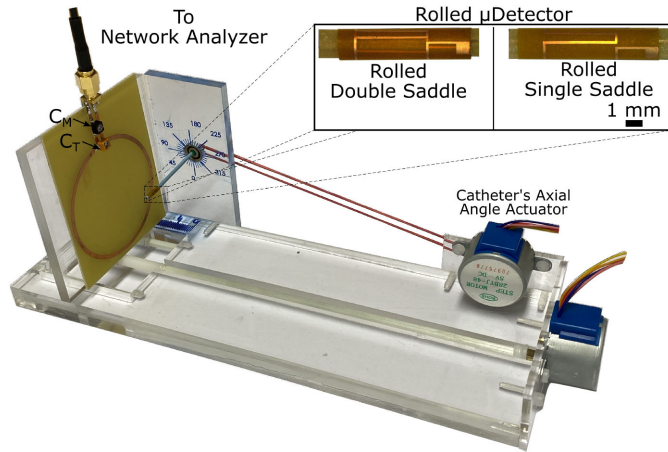


Fig. 8. Experimental setup to characterize the coupling strength between a conventional scale primary coil and a micro detector.

IV. EXPERIMENTAL METHODS AND RESULTS

Two experiments were performed to verify the enhancement provided by the double saddle coil. The first was to characterise the coupling between the surface coil and the micro saddle coil at different relative axial orientations. The second was to map the B_1 field of the saddle coil within an MRI scanner.

A setup was built from laser-cut PMMA to characterise the transmission coefficient between a primary stationary surface coil and a micro saddle coil immobilised on a catheter tip, as shown in Fig. 8. The primary coil ($r = 2$ cm) was connected to a network analyser through a circuit containing variable capacitors for matching and tuning. The catheter was adjusted so that its tip faced the centre of the primary coil at a distance of 2 cm. Its axial orientation was controlled using a stepper motor actuator. The experiment was performed once with a single saddle coil, and subsequently with a double saddle coil. The primary surface coil was matched and tuned to 63 MHz. The single saddle coil had an inductance of 16 nH and was tuned by a 390 pF capacitor (SMD capacitor 0402) to $f_0 = 63$ MHz, while the double saddle coil was tuned by a 190 pF capacitor to the same resonance frequency. The reflection coefficient (S_{11}) of the primary coil was recorded at different relative axial orientations with the micro-coil immobilised on the catheter's tip.

The practical results of the coupling characterization is shown in Fig. 9, which matches with the simulation results in Fig. 5

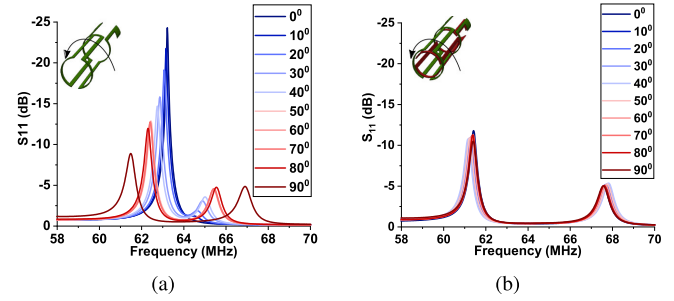


Fig. 9. Reflection coefficient curves of the primary coil show characteristic frequency splitting due to inductive coupling. (a) Single saddle coil. (b) Double saddle coil.

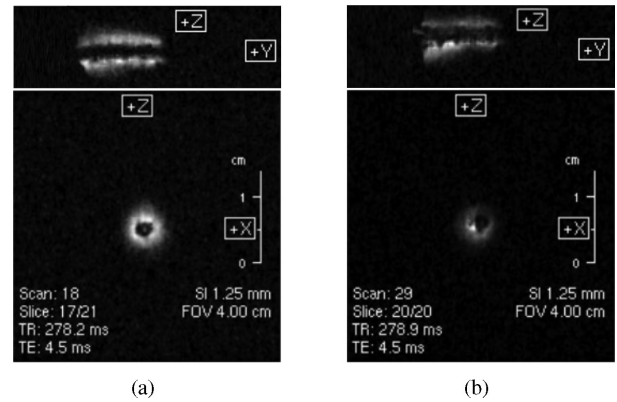


Fig. 10. Mapping the B_1 field using a low field scanner at a single orientation. (a) Double saddle coil. (b) Single saddle coil.

b, where the coupling between the single saddle coil and the primary coil decreased as the angle between their magnetic fields B_1 increased. When the fields were nearly orthogonal, the curve showed no splitting in frequency, confirming that no coupling occurred. For the double saddle coil, the coupling between the coils was maintained at a near constant profile through the entire range of axial orientations.

The magnetic field of the saddle coils was mapped using a low field MRI scanner (Bruker ICON, $B_0 = 1$ T). As shown in Fig. 10, a homogeneous distribution of the field, generated by the double saddle coil around the catheter tube, was observed, confirming the simulated magnetic field in Fig. 4. The MR image had a field of view of 20 mm * 20 mm, and a slice thickness of 1.25 mm, with an imaging matrix size set as (128 * 128) using TE = 4.5 m sec, TR = 278 m sec, a flip angle of 40 deg, and using 4 averages. For the single saddle coil, the strongest signal was obtained at TR=264m sec.

V. CONCLUSION

A double saddle detector design was proposed for orientation independent wireless tracking of an MR-catheter for use during interventional magnetic resonance imaging (iMRI) operation. The performance of the double saddle detector was compared to that of a conventional single saddle coil using numerical simulations and confirmed by experiments.

The B_1 fields generated by the coils were simulated using COMSOL multiphysics, and were mapped in a low field MRI scanner (Bruker ICON, $B_0 = 1$ T). The magnetic field generated by the double coil was found to be distributed homogeneously entirely around the coil.

The coupling between the micro detector and a larger surface coil was also simulated using COMSOL Multiphysics. In addition, a home-built setup was used to characterise the coupling strength between the micro detectors and a surface coil. The double detector showed constant coupling through the entire range of axial orientations. The coupling of the single detector with the surface coil decreased as the angle between their magnetic fields increased, and were completely decoupled when their fields were orthogonal.

A new two multi-layer fabrication process for rolled MEMS was introduced. One process used inkjet printing, the other was based on standard lithography micro fabrication and a via process step. Both processes were successfully used to fabricate double saddle resonators, which were rolled around a 5 fr ≈ 1.667 mm catheter tube before testing.

APPENDIX

The Kirchhoff law states that the individual loop equations of two inductively coupled resonators are zero, i.e., $Z_1 I_1 + j\omega M I_2 = 0$ and $Z_2 I_2 + j\omega M I_1 = 0$ [23]. Solving the loop equations simultaneously results in two resonance frequencies. When substituting $\omega_{01} = \omega_{02} = \omega_0$, (1) can be deduced.

REFERENCES

- [1] H. Ritchie and M. Roser, "Causes of death," *Our World in Data*, 2020, <https://ourworldindata.org/causes-of-death>
- [2] K. Pushparajah, H. Chubb, and R. Razavi, "Mr-guided cardiac interventions," *Topics Magn. Reson. Imag.*, vol. 27, no. 3, pp. 115–128, 2018.
- [3] M. J. Kern *et al.*, "Physiological assessment of coronary artery disease in the cardiac catheterization laboratory: A scientific statement from the american heart association committee on diagnostic and interventional cardiac catheterization, council on clinical cardiology," *Circulation*, vol. 114, no. 12, pp. 1321–1341, 2006.
- [4] F. A. Jolesz and S. M. Blumenfeld, "Interventional use of magnetic resonance imaging," *Magn. Reson. Quart.*, vol. 10, no. 2, pp. 85–96, 1994.
- [5] T. Rogers and R. J. Lederman, "Interventional CMR: Clinical applications and future directions," *Current Cardiology Rep.*, vol. 17, no. 5, p. 31, 2015.
- [6] M. R. Prince, E. K. Yucel, J. A. Kaufman, D. C. Harrison, and S. C. Geller, "Dynamic gadolinium-enhanced three-dimensional abdominal MR arteriography," *J. Magn. Reson. Imag.*, vol. 3, no. 6, pp. 877–881, 1993.
- [7] K. Ratnayaka, A. Z. Faranesh, M. A. Guttman, O. Kocaturk, C. E. Saikus, and R. J. Lederman, "Interventional cardiovascular magnetic resonance: Still tantalizing," *J. Cardiovascular Magn. Reson.*, vol. 10, no. 1, p. 62, 2008.
- [8] O. Ocali and E. Atalar, "Intravascular magnetic resonance imaging using a loopless catheter antenna," *Magn. Reson. Medicine*, vol. 37, no. 1, pp. 112–118, 1997.
- [9] E. Larose *et al.*, "Characterization of human atherosclerotic plaques by intravascular magnetic resonance imaging," *Circulation*, vol. 112, no. 15, pp. 2324–2331, 2005.
- [10] C. L. Dumoulin, S. Souza, and R. Darrow, "Real-time position monitoring of invasive devices using magnetic resonance," *Magn. Reson. Medicine*, vol. 29, no. 3, pp. 411–415, 1993.
- [11] E. Atalar *et al.*, "High resolution intravascular MRI and MRS by using a catheter receiver coil," *Magn. Reson. Medicine*, vol. 36, no. 4, pp. 596–605, 1996.
- [12] S. Wildermuth, C. L. Dumoulin, T. Pfammatter, S. E. Maier, E. Hofmann, and J. F. Debatin, "Mr-guided percutaneous angioplasty: Assessment of tracking safety, catheter handling and functionality," *Cardiovascular Interventional Radiol.*, vol. 21, no. 5, pp. 404–410, 1998.

- [13] M. E. Ladd and H. H. Quick, "Reduction of resonant RF heating in intravascular catheters using coaxial chokes," *Magn. Reson. Medicine: An Official J. Int. Soc. Magn. Reson. Medicine*, vol. 43, no. 4, pp. 615–619, 2000.
- [14] M. Schnall, C. Barlow, V. H. Subramanian, and J. Leigh Jr, "Wireless implanted magnetic resonance probes for in vivo NMR," *J. Magn. Reson.*, vol. 68, no. 1, pp. 161–167, 1986.
- [15] H. H. Quick *et al.*, "Interventional magnetic resonance angiography with no strings attached: Wireless active catheter visualization," *Magn. Reson. Medicine: An Official J. Int. Soc. Magn. Reson. Medicine*, vol. 53, no. 2, pp. 446–455, 2005.
- [16] H. H. Quick, H. Kuehl, G. Kaiser, S. Bosk, J. F. Debatin, and M. E. Ladd, "Inductively coupled stent antennas in MRI," *Magn. Reson. Medicine: An Official J. Int. Soc. Magn. Reson. Medicine*, vol. 48, no. 5, pp. 781–790, 2002.
- [17] T. Kuehne, R. Fahrig, and K. Butts, "Pair of resonant fiducial markers for localization of endovascular catheters at all catheter orientations," *J. Magn. Reson. Imag.: An Official J. Int. Soc. Magn. Reson. Medicine*, vol. 17, no. 5, pp. 620–624, 2003.
- [18] F. E. Terman, *Radio Engineers' Handbook*. New York, NY, USA: McGraw-Hill, 1943.
- [19] N. Wang, M. Meissner, N. MacKinnon, V. Luchnikov, D. Mager, and J. Korvink, "Fast prototyping of microtubes with embedded sensing elements made possible with an inkjet printing and rolling process," *J. Micromechanics Microengineering*, vol. 28, no. 2, p. 025003, 2017.
- [20] H. Sirringhaus *et al.*, "High-resolution inkjet printing of all-polymer transistor circuits," *Science*, vol. 290, no. 5499, pp. 2123–2126, 2000.
- [21] O. Nassar, D. Mager, and J. G. Korvink, "A novel sensor design and fabrication for wireless interventional MRI through induction coupling," in *Proc. IEEE SENSORS*, 2019, pp. 1–4.
- [22] O. Nassar, M. V. Meissner, S. Wadhwa, J. G. Korvink, and D. Mager, "Load sensitive stable current source for complex precision pulsed electroplating," *Rev. Scientific Instrum.*, vol. 90, no. 10, p. 104704, 2019.
- [23] N. Balabanian, *Electric Circuits*. New York, NY, USA: McGraw-Hill, 1994.



Omar Nassar received the B.Sc. (Hons.) and M.Sc. degrees in mechatronics engineering from Ain Shams University, Cairo, Egypt, in 2011 and 2015, respectively. He is currently working toward the Ph.D. degree with Karlsruhe Institute of Technology, Karlsruhe, Germany. His thesis focuses on the development of microresonator and embedded systems for safe and reliable interventional Magnetic Resonance Imaging (iMRI). His research interest includes sensor systems, microfabrication, and embedded systems.



Dario Mager received the Diploma in MEMS, and the Ph.D. degree on the topic of fabrication of microstructures using inkjet printing, from the University of Freiburg (IMTEK), Freiburg im Breisgau, Germany. Today he runs the low-cost MEMS group at the Institute of Microstructure Technology (IMT) at the Karlsruhe Institute of Technology, Karlsruhe, Germany. With his team he works on MEMS devices that can be fabricated without a cleanroom. The naturally lower level of quality is compensated by using embedded systems for a better signal

readout and analysis.



Jan G. Korvink (Senior Member, IEEE) received the M.Sc. degree in mechanical engineering from the University of Cape Town, South Africa, in 1987, and the Ph.D. degree from the ETH-Zurich, Switzerland, in 1993. In 1997 he joined the University of Freiburg, Germany, as Full Professor for microsystems engineering. He co-directed the Freiburg Institute for Advanced Studies (FRIAS). In 2015 he joined the Karlsruhe Institute of Technology, where he directed the Institute of Microstructure Technology, and acts as a Speaker of the Helmholtz Programme "Science and Technology of Nanosystems". He has coauthored more than 220 journal articles, and was a recipient of a European Research Council Advanced Grant.